Polymer 51 (2010) 3971–3977

Contents lists available at ScienceDirect

Polymer

journal homepage: www.elsevier.com/locate/polymer

# Structure of copolymer films created by plasma enhanced chemical vapor deposition

Someswara R. Peri [a], Hyeonjae Kim [a], Bulent Akgun [a,1], Jesse Enlow [b], Hao Jiang [b], Timothy J. Bunning [b], Xuefa Li [c], Mark D. Foster [a,*]

[a] Institute of Polymer Science and Polymer Engineering, The University of Akron, 170 University Ave., Akron, OH 44325-3909, USA
[b] Air Force Research Laboratory, Materials and Manufacturing Directorate, Wright-Patterson Air Force Base, OH 54333, USA
[c] Advanced Photon Source X-ray Science Division, Argonne National Laboratory, 9700 South Cass Ave, Argonne, IL 60439, USA

ARTICLE INFO

*Article history:*
Received 19 December 2009
Received in revised form
19 June 2010
Accepted 30 June 2010
Available online 7 July 2010

*Keywords:*
Plasma enhanced chemical vapor deposition
Plasma copolymerization

ABSTRACT

The interface structure in copolymer films made using plasma enhanced chemical vapor deposition (PECVD) has been probed for the first time using X-ray reflectivity. Copolymer films made from comonomers benzene (B), octafluorocyclobutane (OFCB), and hexamethyldisiloxane (HMDS) show extremely sharp interfaces and scattering length density depth profiles that are uniform with depth, making them useful for optical applications. The polymer/air interface has an rms roughness (~5 Å) that is only slightly larger than that of the supporting substrate (~3 Å). Addition of either benzene or HMDS as a comonomer in the deposition of OFCB alters a transient deposition behavior at the silicon oxide interface that occurs when using only OFCB. For the B–OFCB copolymer films, a facile control of refractive index with monomer feed composition is achieved. A nonlinear variation in the X-ray scattering length density with composition for the HMDS–OFCB copolymer films is consistent with the nonlinear visible light refractive index (632.8 nm) variation reported earlier.



## 1. Introduction

Increasingly sophisticated devices involving thin films can be fashioned from organic precursor materials using plasma enhanced chemical vapor deposition (PECVD). Such films can be made to have highly crosslinked structures, to be pin-hole free, and to have good adhesion to substrates. In addition, their refractive indices and thicknesses can be controlled. These attractive properties make them useful for a wide variety of potential applications, including optical devices such as narrow notch filters and anti-reflective coatings [1–3]. The refractive index can be tuned to values between or beyond the scope of those of known precursors by the simultaneous deposition of films from two monomer precursors to form materials we refer to here, for convenience, as "copolymers." Jiang et al. [1,4] demonstrated the ability to control the refractive index profile and optical thickness for photonic coating applications by adjusting the comonomer feed ratio and location.

Many of the details of plasma polymerization with one or more precursors remain unclear, so defining relationships among process parameters, structure, and properties remains a key objective in studies of PECVD films. Hirotsu et al. [5] found that plasma power is the key parameter in controlling chemical composition and morphology of copolymer films from acrylic acid and hexamethyldisilazane. Copolymer films produced at lower plasma power were hydrophilic, while those produced at higher plasma power were hydrophobic. Beck et al. [6] used plasma copolymerization to generate new surfaces with controlled properties by varying plasma power and monomer flow rate. Other studies in the area of plasma copolymerization [7–12] have focused on the incorporation of different chemical functionalities into the final film and the impact of this incorporation on surface characteristics; however, little work has been done on the physical characteristics of the interfaces in these systems. In this contribution, we report the details of the structure with depth and surface roughness of interfaces of copolymer films.

The present work focuses on copolymer films from benzene (B), hexamethyldisiloxane (HMDS) and octafluorocyclobutane (OFCB) precursors. We address two questions: Can films with a uniform structure throughout the film be deposited using copolymerization? How does copolymerization impact the characteristics of the interfaces with the substrate and air?

To probe the interface structure of PECVD films, we have used X-ray scattering techniques along with atomic force microscopy

* Corresponding author. Tel.: +1 330 972 5323; fax: +1 330 972 5290.
*E-mail address:* mfoster@uakron.edu (M.D. Foster).
[1] Present address: NIST Center for Neutron Research, Gaithersburg, MD 20899, USA.

0032-3861/$ – see front matter © 2010 Elsevier Ltd. All rights reserved.
doi:10.1016/j.polymer.2010.06.055

(AFM). X-ray photoelectron spectroscopy (XPS) determines surface composition which varies with monomer feed [13]. X-ray reflectometry (XR) is sensitive to film thickness, and can resolve variations in composition with depth as well as defining integral interface roughness [14–20] with a resolution of a few Ångstroms. Kim et al. [21] studied with XR and neutron reflectivity the interfaces of PECVD homopolymer films, bilayer films and multilayers made from benzene and OFCB precursors.

While XR has exquisite depth resolution (1–2 nm) for variations in structure normal to the film surface, it provides a global, statistical picture of morphology that is averaged over areas of $mm^2$ in the *x*- and *y*-directions. Therefore, scanning probe microscopy (SPM) imaging, which provides a highly local, direct and laterally resolved characterization of a film surface, is a powerful complement to reflectivity. In the present work AFM and XR measurements of copolymer films of two types of comonomers series show them to have extremely smooth surfaces with rms roughnesses in the range of 2.5–6.4 Å. For all copolymer films the structure also appears to be uniform through the entire thickness of the film. For the B–OFCB (CO-BF) copolymer series made from benzene and OFCB, the refractive index at 632.8 nm increased in a linear fashion (1.4–1.6) with decreasing fluorine content in the film. In the copolymers from HMDS and OFCB (CO-HF) series, a peak in the refractive index at 632.8 nm (1.53) was observed that is higher than the refractive index of either monomer (1.4 for OFCB and 1.47 for HMDS).

## 2. Experimental section

The PECVD system for this study was described elsewhere [4]. For the plasma homo- and co-polymerizations, vapor of the HPLC grade liquid benzene (99.9%, Aldrich [i]), octafluorocyclobutane (OFCB) compressed gas (>99%, SynQuest Laboratories, Inc.), and vapor of the chemical grade hexamethyldisiloxane (HMDS) (>98%, Aldrich) were used as monomers without further purification. The plasma polymerized films were deposited on 2″ silicon wafers. During the depositions, OFCB was always fed into the plasma zone, 17 cm from the substrate position, while the feed position of benzene or HMDS comonomer was downstream, 7 cm beyond the edge of the plasma zone and only 1.5 cm upstream of the substrates.

For the plasma copolymer film deposition of HMDS and OFCB, the processing conditions were plasma power of 40 W, Ar flow rate of 100 $cm^3$/min, and system pressure of 0.75 torr. The HMDS vapor had a flow rate controlled in the range of 0.1–1.18 $cm^3$/min using a high-accuracy metering valve. The OFCB gas had a flow rate of 0.5–5 $cm^3$/min controlled by a flow-controller (Sierra 902C). The copolymer films of OFCB and HMDS were made using volumetric flow rate ratios to yield a series of samples with the Si content increased in roughly regular increments from 0 atom% (pure OFCB) to 25.8 atom% (pure HMDS). We denote such copolymer films with the abbreviation “CO-HFXX”, with “H” denoting the HMDS comonomer, “F” denoting the OFCB comonomer, and the ending digits “XX” indicating Si atom% in the film.

For the plasma copolymer film deposition of benzene and OFCB, the processing conditions were plasma power of 30 W, Ar (noble gas) flow rate of 100 $cm^3$/min, and system pressure of 0.6 torr. The benzene vapor flow rate was controlled by a manually adjusted high-accuracy metering valve in the range of 0.004–0.3 $cm^3$/min. OFCB gas was fed as with the other type of copolymerization. A series of plasma-copolymerized benzene–OFCB films were made by adjusting the volumetric flow rate ratios to yield a specific fluorine content. The F content was increased in roughly regular increments from 0 atom% (pure benzene) to 63 atom% (pure OFCB). The sample notation “PP-OFCB” indicates a homopolymer film made from OFCB precursor, and “CO-BF10” indicates a copolymer film made from benzene and OFCB monomers with the ending digits in the sample name indicating the fluorine content in the film, i.e. a fluorine content of 10 atom%.

Actual Si content was determined using a Surface Science Instruments M-probe spectrometer equipped with a monochromatic Al $K_\alpha$ source producing X-rays with an energy of 1486.6 eV. Survey scans covering binding energies between 0 and 1000 eV were used to determine overall surface composition. The spectrometer resolution was 1.5 eV and the analysis area was approximately 400 μm × 1000 μm. Measurements were taken at the center and at the edge of each sample, using an incidence angle of 30° from the sample surface.

XR measurements were performed at the 1-BM beamline ($\lambda = 1.24$ Å) at the Advanced Photon Source or using a spectrometer mounted on a rotating anode source [22] (Rigaku, 12 kW RU200) with Cu $K_\alpha$ radiation ($\lambda = 1.54$ Å). Reciprocal space resolution $\delta q_z$ in both instances was 0.001 $Å^{-1}$. Background scattering was measured using longitudinal diffuse scans in which the detector and incident angles were increased simultaneously, but with the incident angle offset by 0.1° from the specular condition. This background intensity was subtracted from the measured specular intensity to yield the true specular intensity [23]. Our experience with measuring the films both for this study and for other synchrotron X-ray studies revealed that the films are quite resistant to damage by an X-ray beam and certainly more resistant than spun-cast polystyrene films for which the main mechanism of beam damage is crosslinking at room temperature and chain scission at temperatures above the glass transition temperature ($T_g$) [24]. In both cases, radiation damage to the film structure can be detected by comparing consecutive reflectivity runs. If beam damage causes chain scission, the film gets thinner and the air interface becomes rougher, while crosslinking causes an increase in film thickness and a slight reduction in roughness at the air interface. Collecting reflectivity curves twice from the same sample location, even with synchrotron radiation, revealed no change in the curve for all the homopolymer and copolymer films measured in this study.

AFM imaging was done on a Dimension 3100 Scanning Probe Microscope using tapping mode with a noncontact silicon tip (NSC 16). The images were corrected for curvature due to bending of the scanner. After film thicknesses had been precisely defined using XR, the refractive index of each film was determined using ellipsometry measurements on a Gaertner model L116C equipped with a He–Ne laser ($\lambda = 632.8$ nm) and a fixed incident angle of 70°.

## 3. Results and discussion

### 3.1. Interface structure of HMDS–OFCB copolymer films

The X-ray data for the HMDS–OFCB copolymer film series, including the “homopolymer” films, are presented in Figs. 1–3. The most evident differences among the reflectivity curves are the differences in spacing of the interference fringes, indicative of the film thicknesses. No attempt was made to keep the thicknesses of various films the same; thicknesses vary from film to film. However, in each case the thickness can be precisely determined from the data, and in our thickness range, no evidence was found that the interface structure varied with thickness.

Details of the film structure in each case were obtained by nonlinear regression of the data. A parameterized model of the film structure was assumed, the reflectivity curve expected from such a film calculated and compared to the data, and then the parameters varied until the best agreement between model and data was achieved [23]. Such a fitting procedure is unable to provide a structural solution that is mathematically unique. However, using

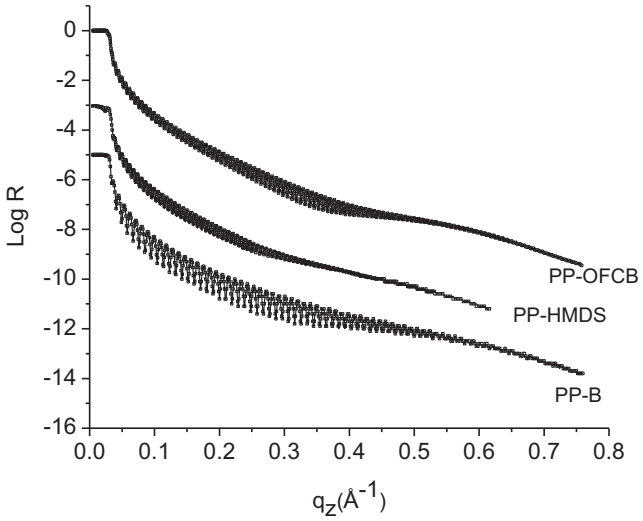


**Fig. 1.** Synchrotron XR data (open squares) for PP-OFCB, PP-HMDS and PP-B homopolymer films and best fits (solid line). Data for PP-HMDS and PP-B offset for clarity.

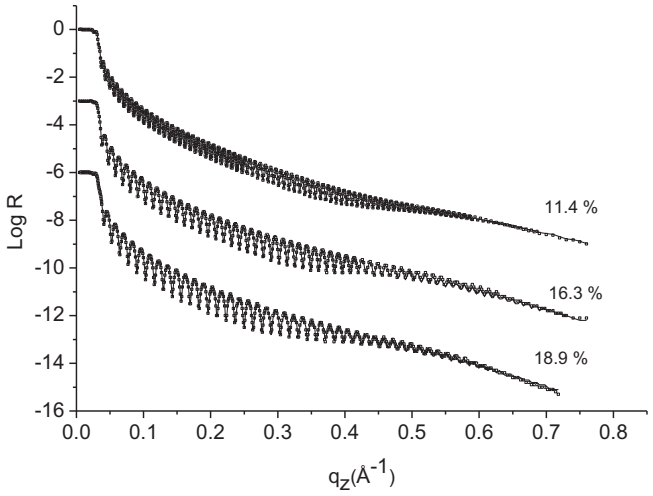


**Fig. 3.** Synchrotron XR data (open squares) for three CO-HF films with various Si contents and the best fit (solid line) to each data set. Data for 16.3 and 18.9% offset for clarity.

knowledge of how the sample was made and constraining the fits from all data to conform to a consistent picture of the film structure gives substantial confidence that the parameter values so derived reasonably describe the actual structure. The one-dimensional structural model is constructed by first envisioning a stack of layers, with each layer having uniform scattering length density (SLD). X-ray SLD, or $(b/V)_x$ is the property of the sample to which the reflectometry measurement is sensitive. The density of scattering length $(b/V)$, is related to the electron density, $\rho_e$, by

$$(b/V)_x = r_e\rho_e \tag{1}$$

$$\rho_e = \frac{N_A\rho_b\sum b_i}{MW} \tag{2}$$

where $r_e$ is the classical electron radius, $\rho_b$ is the mass density, $N_A$ is the Avogadro's number, $\sum b_i$ is total scattering length in a representative 'structural unit' and is given (for a wavelength far from an absorption edge) by the sum of atomic numbers $(Z_i)$ of the atoms in that structural unit, and $MW$ is the molecular weight of that structural unit.

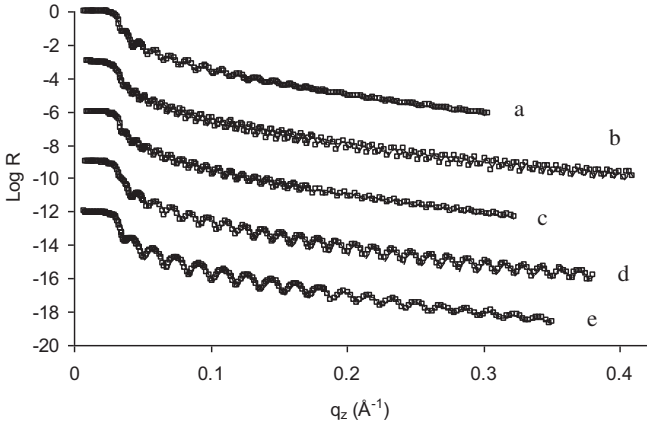


**Fig. 2.** XR data, measured using the rotating anode source, for CO-HF copolymer films with various compositions designated in Si atom% and the best fit (solid line) to each. Their compositions and thicknesses are: a) 3.2%, 471 Å, b) 7.4%, 838 Å, c) 8.1%, 672 Å, d) 9.6%, 460 Å, and e) 10.6%, 351 Å. Each data set except "a" has been shifted by three orders of magnitude from the adjacent data set for clarity.

The parameters used to describe the layer model at this level of sophistication are the thickness $(d)$, roughness $(\sigma)$, and SLD for each layer in the stack. At the bottom of the stack is the silicon substrate, then the native oxide ($SiO_x$), then one or more layers describing the polymer film, and finally the air. Each step function in SLD corresponding to an interface in this initial model is convoluted with an error function of appropriate width to describe the effective interface width due to intrinsic breadth and microroughness. For calculation of the model reflectivity, the SLD profile is discretized and the reflectivity calculated using the Parratt formalism [25]. Parameters of the film structure in each sample corresponding to best fits are given in Table 1. In each case, a good fit with a normalized sum of squared errors, $\chi^2$, less than 0.7 was obtained. The precision with which the SLD of the film is determined by the fitting procedure is very good, of order $0.1 \times 10^{-6}$ or ca. 1% as indicated in Table 1. The relative precision of the determination of interface width is much lower, with the uncertainty being of order 15–20% for these very small interface widths.

The trends in film characteristics of central interest are the uniformity of composition with depth and the variation in interface roughness with composition. The SLD profiles for the PP-OFCB film, five copolymer films of various compositions, and the PP-HMDS film are shown in Fig. 4. The SLD characteristic of the polymer film varied non-monotonically with copolymer composition and the

**Table 1**
Summary of film structure parameters from XR fitting for CO-HF series.

| Sample Name –Layer | Oxide $d$ (Å)[a] | Oxide $\sigma$ (Å)[a,b] | Bulk $d$ (Å)[a] | Bulk $\sigma$ (Å)[a,b] | $b/V$ ($\times 10^{-6}$ Å$^{-2}$)[a] |
|---|---|---|---|---|---|
| PP-OFCB | 10.6 | 2.6 | 914 | 5.5 | 15.7 |
| Transition | – | – | 5.7 | 3.6 | 14.8 |
| CO-HF3 | 12.3 | 2.4 | 471 | 4.3 | 14.5 |
| CO-HF7 | 12.3 | 2.0 | 838 | 4.8 | 13.5 |
| CO-HF8 | 10.0 | 2.2 | 672 | 4.2 | 13.1 |
| CO-HF9 | 12.5 | 2.2 | 459 | 5.1 | 12.6 |
| CO-HF11 | 11.4 | 2.3 | 351 | 3.9 | 12.5 |
| CO-HF12 | 12.4 | 2.3 | 806 | 4.5 | 12.3 |
| CO-HF16 | 12.5 | 2.7 | 533 | 4.1 | 11.7 |
| CO-HF19 | 10.1 | 2.3 | 467 | 4.6 | 10.1 |
| PP-HMDS | 11.9 | 2.8 | 972 | 6.4 | 8.1 |

[a] Uncertainties inferred from the fitting process are $d$ ±2 Å, $\sigma$ ±15–20%, and $b/V$ $\pm 10^{-7}$ Å$^{-2}$.
[b] The roughness reported for the oxide is for the oxide–polymer interface and that reported for the bulk is for the polymer–air interface.

SLD profile was uniform with depth for all the HMDS–OFCB copolymer films. Hence, for clarity only profiles for five of the eight copolymer films are shown. For the PP-OFCB homopolymer film, it was necessary to include in the model a transition layer between the oxide layer and the layer describing the bulk of the polymer film. Such a transition layer was observed first for a PP-OFCB film by Kim et al. [22]. They argued that the structure resulting from the deposition of reactive fragments on oxide differs from the structure resulting from deposition on previously formed polymer. The fact that the transition in structure occurs over such a small depth, ca. 10 Å, suggests that only a single layer of organic fragments deposited at the surface is necessary to substantially screen the influence of the oxide as far as surface chemical reactivity is concerned. For the eight copolymer films and the HMDS homopolymer film, no transition layer adjacent to the oxide is required in order to fit the data well. Fitting using a model with a transition layer was also tried, but this offered no improvement in the fit. Thus, with the present feed geometry even the presence of a small amount of HMDS monomer is sufficient to eliminate the transition layer and deposition of HMDS fragments is less sensitive to whether the deposition is on oxide or an already growing polymer layer than is the deposition of OFCB fragments. Etching of $SiO_2$ by fluorocarbon precursors has been studied extensively in the semiconductor industry due to its applications in lithography, silicon texturisation, microelectronics circuit fabrication, and ultra large scale integrated circuits [26–29]. Several studies have pointed out the formation on the $SiO_2$ surface of an ultrathin film containing mostly carbon rich structure (C–C bonds and C–O bonds) [30–32]. The etch reaction between the $SiO_2$ interface and the incoming fluorine species begins with the formation of a $SiO_2C_xF_y$ complex, which then undergoes dissociation to release products like $COF_y$, $SiF_3$, and $SiF_4$ as volatile etch products [32]. When hydrogen or hydrogen containing precursors are used as comonomers along with fluorocarbon precursors, the etching rate of $SiO_2$ is drastically reduced due to dilution of the fluorine species, which is the main etchant [33–36]. We conjecture that when HMDS is added to the precursor feed, the rate at which the substrate surface is etched is reduced and therefore, since it is an interplay between etching and film deposition that leads to the transition layer, the transition layer disappears. With the transition layer being so thin (few Å), even subtle changes in etching rate will impact the film structure immediately adjacent to the substrate. An alternative explanation that we cannot exclude is that, since the comonomer feed is much closer to the substrate, although the two monomer feeds are initiated simultaneously, the first species striking the sample are all fragments from the comonomer and therefore when the first OFCB fragments arrive they meet an organic, rather than oxide, surface. The net effect would be the same. Any role of etching in determining the film structure immediately adjacent to the substrate is strongly weakened or eliminated.

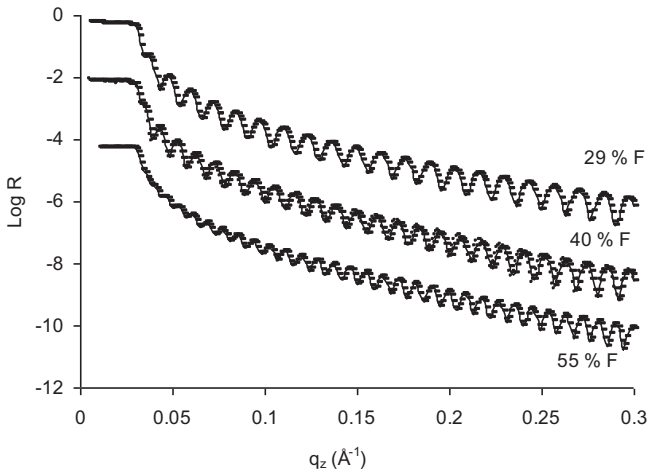


**Fig. 5.** XR data (open squares) for three CO-BF films with varying composition of fluorine as marked. A best fit (solid line) is shown for each data set.

For a polymer film of several hundred Ångstroms thickness analysis of the XR curve can provide the value of the SLD of the film independent of an estimate of thickness through fitting of the critical angle of reflection of the film, as described by Kim et al. [22]. The value of 1.93 g/cm$^3$ found here for the mass density of the PP-OFCB film agrees within experimental error (±0.06 g/cm$^3$) with that reported by Kim et al. [22].

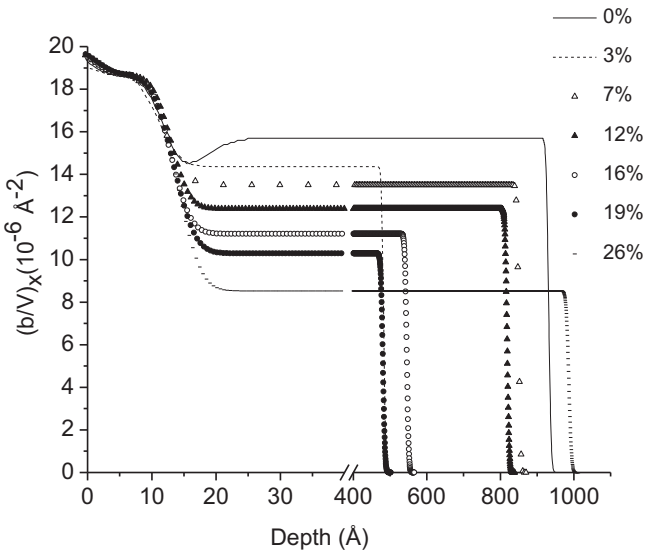


**Fig. 4.** SLD profiles for PP-OFCB, CO-HF3, CO-HF7, CO-HF12, CO-HF16, CO-HF19 and PP-HMDS samples. The depth axis for each data set has been adjusted slightly so that the oxide/film interface profiles for all samples lie on top of one another at one point. The width of that interface varies little from sample to sample.

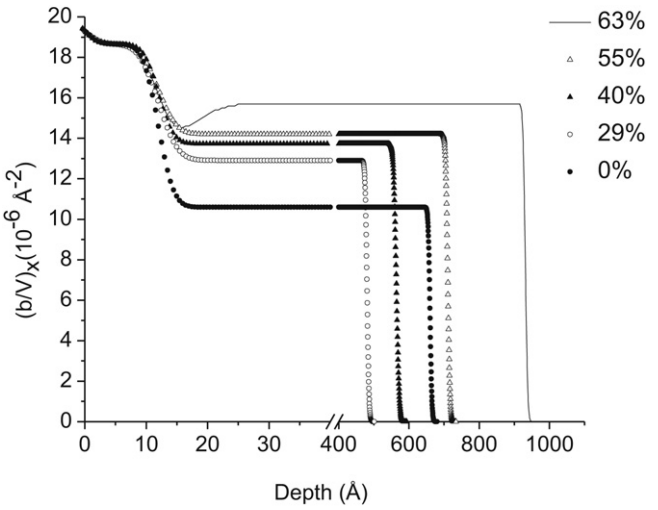


**Fig. 6.** Scattering length density profiles for PP-B, three CO-BF films, and PP-OFCB marked with fluorine contents in atom%. The depth axis for each data set has been adjusted slightly so that the oxide/film interface profiles for all samples lie on top of one another at one point. The width of that interface varies little from sample to sample.

**Table 2**
Summary of film structure parameters for CO-BF series.

| Sample Name – Layer | Oxide $d$ (Å)[a] | Oxide $\sigma$ (Å)[a,b] | Bulk $d$ (Å)[a] | Bulk $\sigma$ (Å)[a,b] | $b/V$ ($\times 10^{-6}$ Å$^{-2}$)[a] |
|---|---|---|---|---|---|
| PP-OFCB | 10.6 | 2.6 | 914 | 5.5 | 15.7 |
| Transition | – | – | 5.7 | 3.6 | 14.8 |
| CO-BF55 | 13.0 | 2.0 | 695 | 3.6 | 14.3 |
| CO-BF40 | 11.0 | 2.0 | 552 | 5.3 | 13.9 |
| CO-BF29 | 12.3 | 2.5 | 466 | 3.9 | 12.7 |
| PP-B | 12.4 | 2.0 | 648 | 4.3 | 10.6 |

[a] Uncertainties inferred from the fitting process are $d$ ±2 Å, $\sigma$ ±15–20%, and $b/V$ $\pm 10^{-7}$ Å$^{-2}$.
[b] The roughness reported for the oxide is for the oxide–polymer interface and that reported for the bulk is for the polymer–air interface.

### 3.2. Interface structure of B–OFCB copolymer films

The X-ray data and best fit for the benzene film are shown in Fig. 1, while those for the B–OFCB copolymer films are presented in Fig. 5. In both figures, the data and fits are only shown to a $q_z$ value of 0.3 Å$^{-1}$ to make the figures clearer, though data were collected and fit to higher values of $q_z$. While the composition of F was systematically varied from 0 atom% to 63 atom%, no attempt was made to achieve the same thickness for every film. The SLD profiles for the three copolymer films (CO-BF55, CO-BF40 and CO-BF29) and the corresponding homopolymer films are shown in Fig. 6 and the parameter values corresponding to all the best fit profiles are summarized in Table 2. In contrast to the case of the PP-OFCB homopolymer film, no transition layer is seen in the SLD profile for the PP-B film.

In B–OFCB copolymer films, the polymer region of the sample is well described by a single layer of uniform SLD, as illustrated in Fig. 6. Each structural model contained model layers for the silicon substrate, a native oxide layer and the polymer film. This behavior is consistent with that of HMDS–OFCB copolymer films, showing that the elimination of the transition layer through the co-deposition of a second monomer with that of OFCB is not peculiar to HMDS.

### 3.3. Optical properties of copolymer films

Another key concern is how the optical properties of the films vary with their composition and structure. The quantity controlled in the deposition is "feed ratio", which, for the CO-HF series, is operationally defined as (volumetric flow rate of OFCB)/(volumetric flow of OFCB + volumetric flow of HMDS). Fig. 7 shows how the Si, F, O, and C elemental compositions of the films vary with feed ratio for this series. Using such information one can then deduce the variation in film refractive index with composition as well as feed ratio. As seen in Fig. 8, for the CO-BF series the refractive index changes linearly with fluorine composition, changing from 1.414 for the PP-OFCB homopolymer to 1.62 for the PP-B homopolymer. After converting from feed ratio to composition one finds that this linear change with composition is consistent with the observations of Jiang et al. [4], which are also reported as a function of feed ratio.

For the CO-HF series, refractive index changes nonlinearly with fluorine composition (Fig. 8), consistent with the observations of Jiang et al. [37]. In the CO-BF films, the refractive index is primarily dictated by C and F atoms, whereas in the CO-HF series the contributions from Si and O make the overall behavior more complicated. As HMDS is added to feed (and therefore F composition in the film drops) the refractive index first increases, then decreases again. The maximum refractive index observed is 1.53, which is substantially higher than the refractive index of either

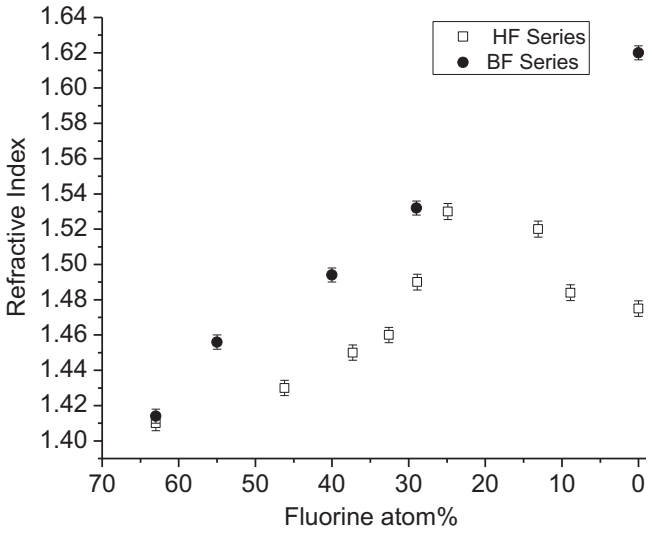


**Fig. 8.** Refractive index at $\lambda = 632.8$ nm versus fluorine atom% for homopolymer OFCB and B, CO-BF series and CO-HF series.

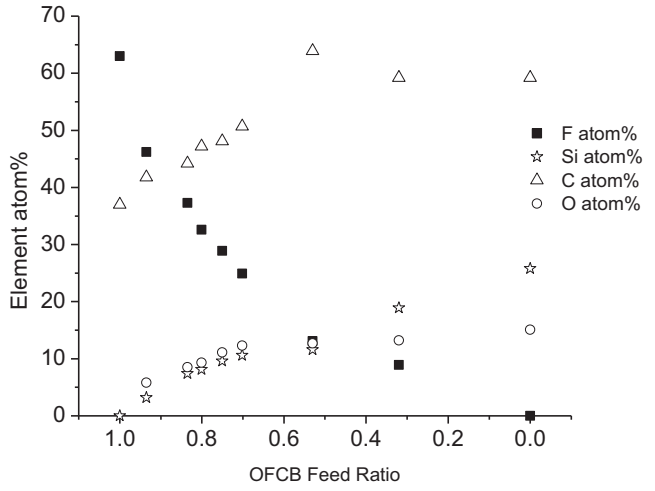


**Fig. 7.** Elemental atomic concentrations versus OFCB feed ratio for the CO-HF series.

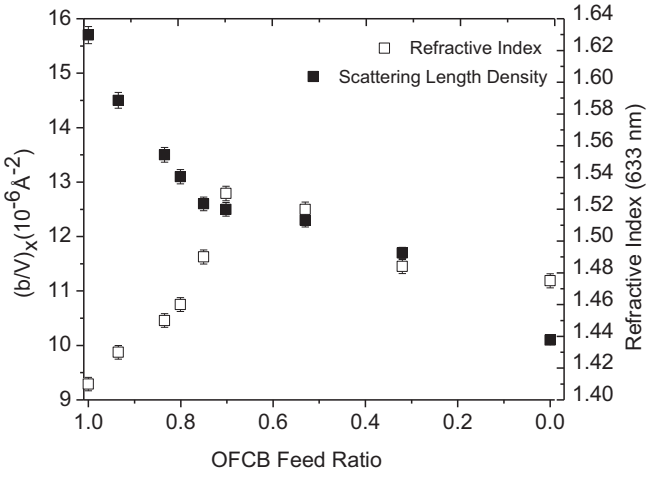


**Fig. 9.** XR SLD and refractive index (at 632.8 nm) versus OFCB feed ratio for homopolymer OFCB and HMDS and CO-HF series.

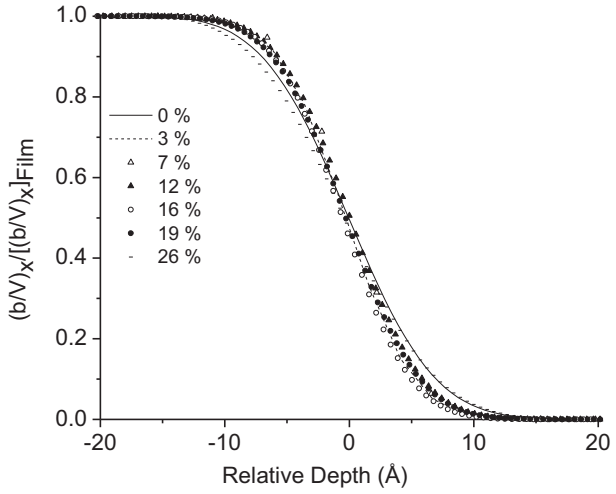


**Fig. 10.** Normalized SLD plotted against relative depth for polymer–air interface of PP-OFCB, CO-HF3, CO-HF7, CO-HF12, CO-HF16, CO-HF19 and PP-HMDS samples.

monomer (OFCB:1.41 and HMDS:1.47), and, it is possible that in the range of fluorine composition between 15 and 25 at%, not yet investigated, the refractive index could be higher still. The initial increase in refractive index can be attributed to the increase in C content and simultaneous decrease in F content. As the OFCB feed ratio drops further (below 0.53) with increasing composition of HMDS in the feed, the carbon content in the film plateaus, while the fluorine content continues to decrease and the silicon and oxygen contents increase.

In Fig. 9 is shown how the "bulk" XR SLD and refractive index (at 632.8 nm) vary with OFCB feed ratio for the CO-HF series. The SLD and refractive index vary nonlinearly with feed ratio and the X-ray scattering length density plateaus around a feed ratio of 0.6 where the optical refractive index passes through a maximum. We conjecture this occurs because in this regime reactions among Si, O, and C atoms begin to become frequent enough that Si–C or Si–O networks can be formed, while for higher OFCB feed compositions a structure characterized by a network of C–C bonds predominates. We conjecture that the change in crosslink network structure from an all carbon network to a network containing silicon results in a less dense film, thus decreasing the refractive index.

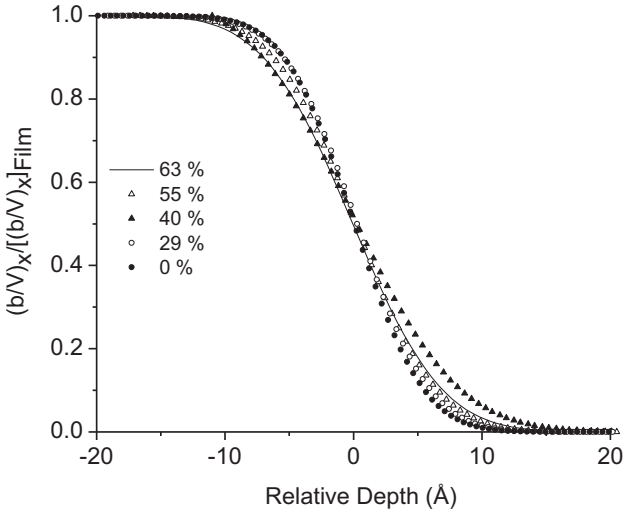


**Fig. 11.** Normalized SLD plotted against relative depth for the polymer–air interface of PP-B, CO-BF29, CO-BF40, CO-BF55, and PP-OFCB marked with fluorine contents in at% as marked.

**Table 3**
Comparison of surface roughnesses measured by XR and AFM for CO-HF and CO-BF series.

| Polymer | Atom% Si[a] | Atom% F[a] | $d$ (Å)[b] | $\sigma_{rms,\ xR}$ (Å)[c] | $\sigma_{rms,\ AFM}$ (Å)[d] |
|---|---|---|---|---|---|
| CO-HF12 | 11.4 | 24.9 | 806 | 4.5 | 3.6 |
| CO-HF16 | 16.3 | 13.1 | 533 | 4.2 | 3.1 |
| CO-HF19 | 18.9 | 8.9 | 467 | 6.4 | 5.2 |
| CO-BF55 | – | 55 | 695 | 5.2 | 2.6 |
| CO-BF40 | – | 40 | 552 | 6.3 | 5.3 |
| CO-BF29 | – | 29 | 466 | 4.3 | 3.9 |

[a] Uncertainties in compositions: ±15% for each.
[b] Uncertainty in $d = \pm 2$ Å.
[c] Uncertainty in $\sigma_{rms/xR} = 10–15\%$.
[d] Uncertainty in $\sigma_{rms/AFM} = \pm 1$ Å.

### 3.4. Comparison of interface widths

The interface between the polymer and air is very smooth for all the samples, with rms roughnesses (~5 Å) only slightly larger than that of $SiO_x$ (~3 Å). That is, the air interface quality is just as good for the copolymer films as for the homopolymer films as shown in Figs. 10 and 11. The substrate/polymer and polymer/air interfaces in PP-films are extremely sharp and the interface widths are comparable to those seen in spun-cast polymer films [38,39].

The roughnesses of all the samples were measured with AFM as well. Images of size 2 μm × 2 μm collected in Tapping Mode revealed extremely smooth surfaces with an rms roughness measured over the entire scan area of 5 Å and similar texture was present at different spots across the surface. We observed similar behavior for all the copolymer films, both those made with benzene and those made with HMDS. A comparison of the sample surface roughnesses determined by XR and AFM is shown in Table 3. In general, the values obtained for roughness by XR and AFM are close for a given sample. Since the range of roughness frequencies to which XR is sensitive is larger than that to which AFM images of this resolution are sensitive, and both roughnesses represent integral values over a range of frequencies, one expects to find somewhat higher roughness from XR data.

## 4. Conclusion

From this study of copolymer films made from OFCB, B and HMDS precursors three major conclusions can be drawn. First, the surfaces of the copolymer films are exceptionally smooth, with rms roughnesses in the range of 3–6 Å, and in the range of thicknesses studied so far (467–942 Å) are comparable in homogeneity to the surfaces of films of either corresponding "homopolymer". Inferences drawn from the XR data are supported by AFM measurements. Second, for all the copolymer films, the polymer structure is characterized by uniform SLD through the depth of the film. The very thin transition layer seen for homopolymer PP-OFCB films is eliminated by copolymerization with a small fraction of either benzene or HMDS. Such uniformity with depth and extremely sharp interfaces make these films very promising for optical applications. Third, a facile control of refractive index is demonstrated which could allow one to fabricate films of arbitrarily complex refractive index profile using computer controlled feed composition and mixed monomers. Such structures would be useful, for example, for photonic applications.

## Acknowledgements

SP thanks Sergei Lyuksyutov for help in doing AFM measurements and John Grant for help with XPS measurements. This research was funded by the Collaborative Center for Polymer

Photonics (49620-02-1-0428) which is co-funded by the Air Force Office of Scientific Research, Air Force Research Laboratory, and The University of Akron. The authors appreciate access to beamline 1-BM and the assistance of Jin Wang and the SRI collaborative access team. Use of the Advanced Photon Source was supported by the U. S. Department of Energy, Office of Science, Office of Basic Energy Sciences, under Contract No. DE-AC02-06CH11357.

## References

[1] Grant JT, Jiang H, Tullis S, Johnson WE, Eyink K, Fleitz P, et al. Vacuum 2005;80 (1–3):12.
[2] Benitez F, Martinez E, Galan M, Serrat J, Esteve J. Surf Coat Technol 2000;125 (2–3):383.
[3] Dilsiz N, Akovali G. Polymer 1996;37(2):333.
[4] Jiang H, O'Neill K, Grant JT, Tullis S, Johnson WE, Eyink K, et al. Chem Mater 2004;16(7):1292.
[5] Hirotsu T, Tagaki C, Partridge A. Plasmas Polym 2002;7(4):353.
[6] Beck JA, Jones RF, Short DR. Polymer 1996;37(24):5537.
[7] Lopattananon N, Hayes AS, Jones RF. Proc Int Conf Fibre Reinforced Composites 2000:345.
[8] Yoshimura K, Minaguchi T, Nakano H, Tatsuta T, Tsuji O. J Photopolym Sci Technol 2001;13(2):13.
[9] Chen R, Silverstein MS. J Polym Sci Part A Polym Chem 1996;34(2):207.
[10] Tsuji O, Minaguchi T, Nakano H. Thin Solid Films 2001;390(1–2):159.
[11] Daw R, O'Leary T, Kelly J, Short RD, Cambray-Deakin M, Devlin AJ, et al. Plasmas Polym 1999;4(2/3):113.
[12] Golub MA, Wydeven T, Finney LS. Polym Prepr (Am Chem Soc Div Polym Chem) 1995;36:107.
[13] Jiang H, Grant JT, Tullis S, Eyink K, Fleitz P, Bunning TJ. Polymer 2004;45(25):8475.
[14] Yim H, Kent MS, Matheson A, Stevens MJ, Ivkov R, Satija S, et al. Macromolecules 2002;35(26):973.
[15] Lagomarsino S, Di Fonzo S, Jark W, Muller B, Cedola A, Pelka G. Mater Res Soc Symp Proc 1995;382:381.
[16] Benattar JJ, Schalchli A. Phys Scr 1994;50(2):188.
[17] Geer R, Qadri S, Shashidhar R, Thibodeaux FA, Duran SR. Liq Cryst 1994;16 (5):869.
[18] Ziegler E, Ferrero C, Lamy F, Chapron C, Morawe Ch. Adv X-Ray Anal 2002; 45:345.
[19] Zymierska D, Sobczak E, Godwod K, Miotkowska S. Appl Crystallogr 1998;17:394–7.
[20] Nelson A, Benjamin MW, Oldham J, Fong C, McLean KM, Hartley PG, et al. Langmuir 2006;22(1):453.
[21] Kim H, Foster MD, Jiang H, Tullis S, Bunning TJ, Majkrzak CF. Polymer 2004;45 (10):3175.
[22] Sheller NB, Petrash S, Foster MD, Tsukruk VV. Langmuir 1998;14(16):4535.
[23] Foster MD. Crit Rev Anal Chem 1993;24(3):179.
[24] Richter AG, Gucio R, Shull K, Wang J. Macromolecules 2006;39 (4):1545–53.
[25] Parratt LG. Phys Rev 1954;95:359.
[26] Amrani AE, Tadjine R, Moussa FY. Int J Plasma Sci Eng 2007;2008:371812.
[27] Booth JP, Cunge G, Chabert P, Sadeghi N. J Appl Phys 1999;85:3097.
[28] Fujita K, Ito M, Hori M, Goto T. J Vac Sci Technol A 1999;17:3260.
[29] Sankaran A, Kushner MJ. J Vac Sci Technol A 2004;22:1260.
[30] Goto T, Hori M. Jpn J Appl Phys Part 1 1996;35:6521–7.
[31] Booth JP. Plasma Sourc Sci Tech 1999;8:249.
[32] Sankaran A, Kushner MJ. J Vac Sci Technol A 2004;22:1242.
[33] Coburn JW, Kay E. J Vac Sci Technol 1979;16:407.
[34] Marra DC, Aydil ES. J Vac Sci Technol A 1997;15:2508.
[35] Coburn JW, Winters HF. J Vac Sci Technol A 1979;16:379.
[36] Flamm DL, Donnelly VM. Plasma Chem Plasma Process 1981;1:317.
[37] Jiang H, Eyink K, Grant JT, Enlow J, Tullis S, Bunning TJ. Chem Vapor Deposition 2008;14:286.
[38] Tolan M, Seeck O, Wang J, Sinha SK, Rafailovich MH, Sokolov J. Physica B 2000;283:22.
[39] Tankaka K, Fujii Y, Atarashi H, Akabori K, Hino M, Nagamura T. Langmuir 2008;24:296.